Optimizing Fracture Spacing and Sequencing in Horizontal-Well Fracturing

Nicolas P. Roussel, SPE, and **Mukul M. Sharma,** SPE, University of Texas at Austin

Summary

Horizontal wells with multiple fractures are now commonly used in unconventional (low-permeability) gas reservoirs. The spacing between perforations and the number and orientation of transverse fractures all have a major impact on well production.

The opening of propped fractures results in the redistribution of local Earth stresses. In this paper, the extent of stress reversal and reorientation has been calculated for fractured horizontal wells using a 3D numerical model of the stress interference induced by the creation of one or more propped fractures. The results have been analyzed for their impact on simultaneous and sequential fracturing of horizontal wells.

Our results demonstrate that a transverse fracture initiated from a horizontal well may deviate away from the previous fracture. The effect of the reservoir's mechanical properties on the spatial extent of stress reorientation caused by an opened crack has been quantified. The paper takes into account the presence of layers that bound the pay zone but have mechanical properties different from those of the pay zone. The fracture vertical growth into the bounding layers is also examined.

It is shown that stress interference, or reorientation, increases with the number of fractures created and depends on the sequence of fracturing. Three fracturing sequences are investigated for a typical field case in the Barnett shale: (a) consecutive fracturing, (b) alternative fracturing, and (c) simultaneous fracturing of adjacent wells. The numerical calculation of the fracture spacing required to avoid fracture deviation during propagation, for all three fracturing techniques, demonstrates the potential advantages of alternate fracture sequencing and zipper fracs to improve the performance of stimulation treatments in horizontal wells.

Introduction

For the past few years, most new wells drilled in the Barnett shale and other shale and tight gas plays have been horizontal wells. Slickwater fracturing is the primary technique used to hydraulically fracture these wells. The horizontal well is generally fractured multiple times, one fracture at a time, starting from the toe. More recently, new stimulation techniques have been investigated to improve the reservoir volume effectively stimulated (Mayerhofer et al. 2010). Simultaneous fracturing of two or more parallel adjacent wells, also referred to as simul-fracs or zipper fracs, aims to generate a more-complex fracture network in the reservoir (Mutalik and Gibson 2008; Waters et al. 2009).

When placing multiple transverse fractures in shales, it is crucial to minimize the spacing between fractures in order to achieve commercial production rates and an optimum depletion of the reservoir (Cipolla et al. 2009), but the spacing of perforation clusters is limited by the stress perturbation caused by the opening of propped fractures (Soliman and Boonen 1997). The geometry and width of fractures are strongly influenced by fracture spacing and number because of mechanical interactions (Cheng 2009). The center fractures, subject to the greatest stress interference, may exhibit a decrease in their width and conductivity. Stress distributions and fracture mechanics must be well understood and quantified to avoid screenouts, propagation of longitudinal fractures, or fractures deviating from their orthogonal orientation. The presence of natural fractures also impacts fracture propagation and increases fracture-path complexity, depending on their preferential orientation and on the importance of the net pressure relative to the horizontal-stress contrast (Olson and Dahi-Taleghani 2009).

Previous studies in the literature on fracture-induced stress interference mostly focus on the effect of a single fracture (Siebrits et al. 1998). Using analytical solutions, Soliman and Adams (2004) calculated the effect of multiple fractures on the expected net pressure and the stress contrast. Both quantities increase substantially with the number of sequential fractures and a smaller fracture spacing. The stress field in the horizontal plane and the fracture geometries were numerically calculated on the basis of a displacement discontinuity method for three transverse fractures assuming a homogeneous single-layer formation with the bounding layers not playing any role except to act as barriers to fracture propagation (Cheng 2009). Microseismic measurements have demonstrated the existence of mechanical-stress interference between multiple transverse fractures. This is sometimes referred to as the stress-shadow effect (Fisher et al. 2004). When multiple fractures are propagated simultaneously, the stress shadow can restrict growth in the middle section of the wellbore while favoring growth at the heel or at the toe. Field experience has demonstrated that the optimal cluster spacing to limit fracture interference must be at least 1.5 to 2 times the fracture height (Ketter et al. 2008).

3D Model of Stress Interference Around a Propped-Open Fracture

The results presented here are organized to highlight the important conclusions that we can reach on the basis of the simulations. The validity of numerical simulations is verified through comparison with existing analytical models (Sneddon and Elliot 1946) for simple fracture geometries. The important addition to existing models consists in the evaluation of the impact of the layers bounding the pay zone on the width of the fracture, which eventually affects the stress interference caused by a propped fracture. The identified dimensionless parameters are the fracture aspect ratio (h_f/L_f), the Poisson's ratio of the pay zone (ν_p), the fracture containment (h_p/h_f), and the ratio of Young's moduli (E_b/E_p). Their effects on the stress contrast generated by the propped fracture, and consequently on the spatial extent of the stress-reversal region, are discussed in the following subsections.

Model Formulation. The geometry of the simulated fracture is shown in **Fig. 1.** The model includes the presence of layers bounding the reservoir, and cases where the fracture is not fully contained ($h_f > h_p$) are accounted for. The layers bounding the pay zone may have mechanical properties (E_b, ν_b) differing from those of the pay zone (E_p, ν_p).

The mechanical behavior of the continuous 3D medium is described mathematically by the equations of equilibrium (Eq. 1), the definition of strain (Eq. 2), and the constitutive equations (Eq. 3). The algebraic system of 15 equations for 15 unknowns (six components of stress σ and strain ε, plus the three components of the velocity vector v) is solved at each node using an explicit, finite-difference numerical scheme. The Einstein summation convention applies to indices i, j, and k, which take the values 1, 2, and 3:

$$\sigma_{ij,j} = \rho \frac{\mathrm{d}v_i}{\mathrm{d}t}. \quad (1)$$

This paper (SPE 127986) was accepted for presentation at the SPE International Symposium and Exhibition on Formation Damage Control, Lafayette, Louisiana, USA, 10–12 February 2010, and revised for publication. Original manuscript received 21 November 2009. Revised manuscript received 08 September 2010. Paper peer approved 29 November 2010.

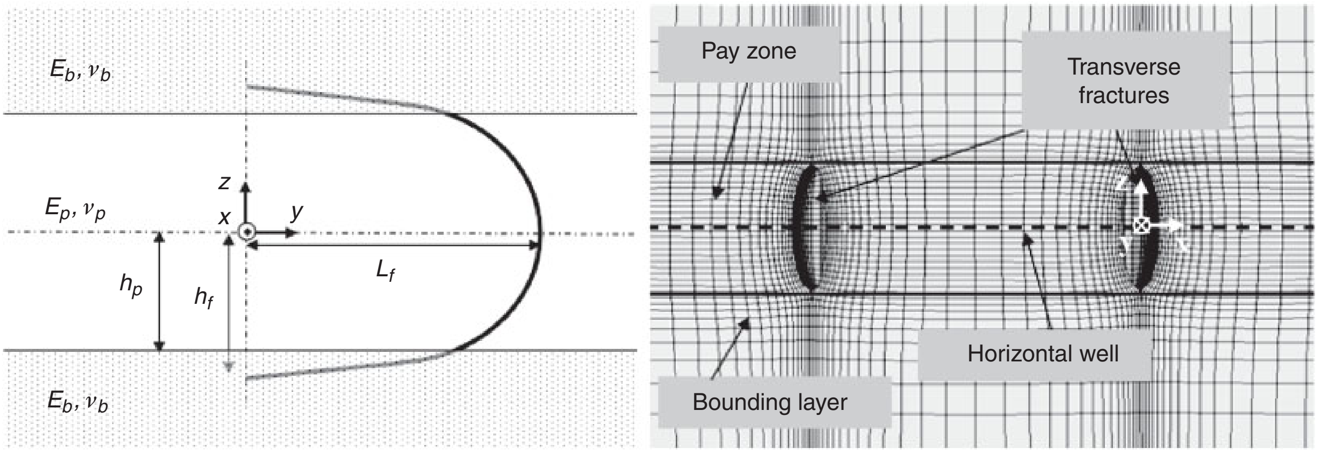

Fig. 1—3D model of multiple transverse fractures in a layered reservoir.

$$\frac{d\varepsilon_{ij}}{dt} = \frac{v_{i,j} + v_{j,i}}{2}. \qquad (2)$$

The pay zone is homogeneous, isotropic, and purely elastic. Hooke's law relates the components of the strain and stress tensors (constitutive equation):

$$\sigma_{ij} = 2G\varepsilon_{ij} + \left(K - \frac{2}{3}G\right)\varepsilon_{kk}\delta_{ij}, \qquad (3)$$

where, $K = \dfrac{E}{3(1-2\nu)}$ and $G = \dfrac{E}{2(1+\nu)}$.

Displacement is allowed along the faces of the fracture where a constant stress, equal to the net pressure p_{net} plus the minimum in-situ horizontal stress S_{hmin}, is imposed. It must be noted that the constant-stress boundary condition on the fracture face is equal to the pressure required to maintain a fracture width w_0, which differs from the pressure during fracture propagation. To avoid an impact on the stress distribution around the hydraulic fracture, the far-field boundaries are placed at a distance from the fracture equal to at least three times the fracture half-length L_f. A constant-stress boundary condition normal to the "block" faces is applied at outside boundaries. In-situ stresses are initialized before the opening of the fracture:

$$\begin{cases} S_{xx} = S_{h\max} \\ S_{yy} = S_{h\min} \\ S_{zz} = S_v \end{cases} . \qquad (4)$$

After the first fracture is created, its geometry is fixed (no displacement is allowed). We assume that compression of the proppant placed inside previous fractures is negligible as a subsequent fracture is opened. Subsequent transverse fractures are modeled using similar boundary conditions **(Fig. 2).** It is observed that the net pressure required to achieve a specified fracture width increases with each additional fracture.

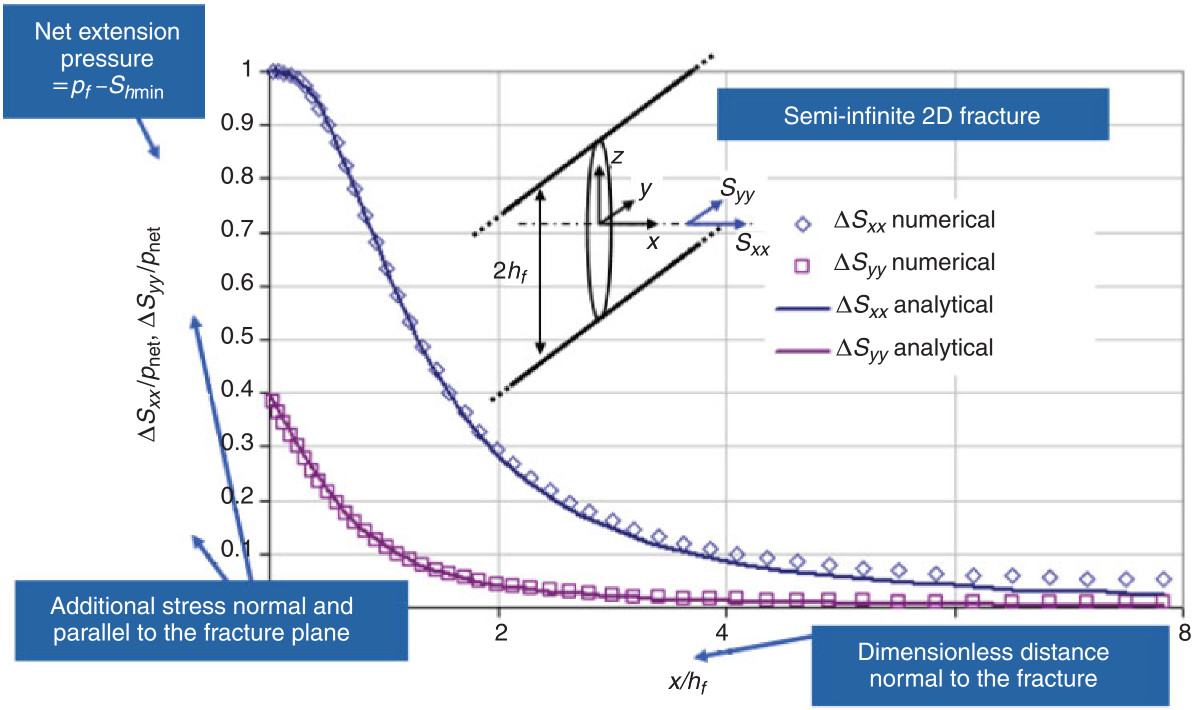

Fig. 2—Comparisons of analytical (Sneddon and Elliot 1946) and numerical additional stresses along a normal (y = z = 0) to a semi-infinite fracture (ν = 0.2).

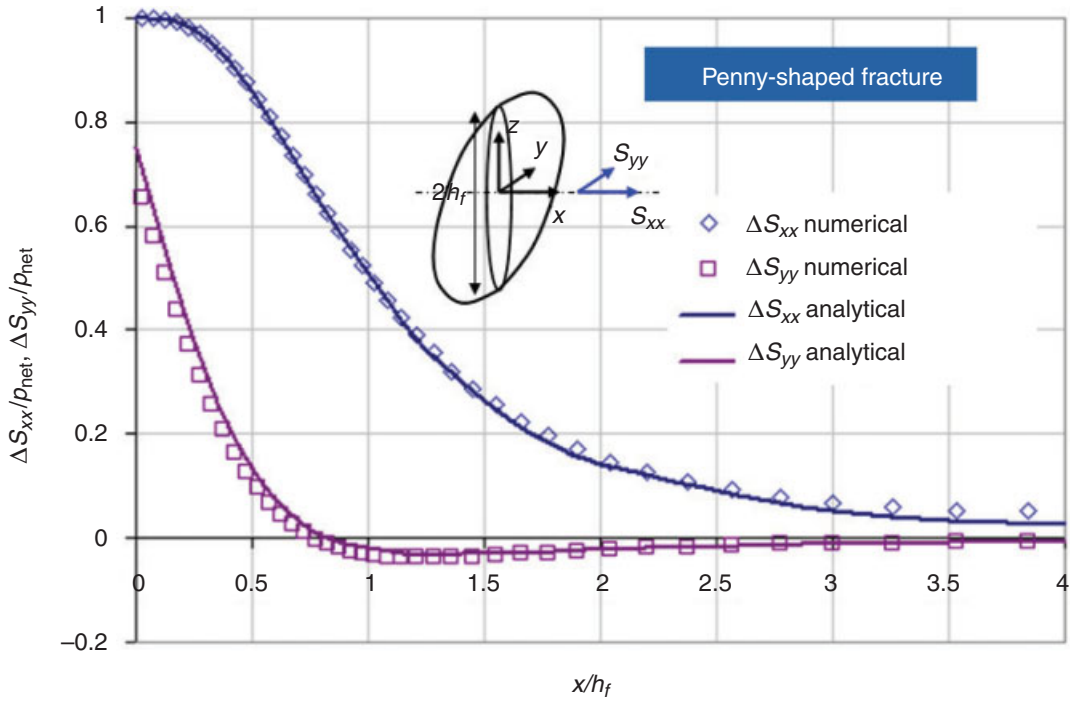

Fig. 3—Comparisons of analytical (Sneddon and Elliot 1946) and numerical additional stresses along a normal ($y = z = 0$) to a penny-shaped fracture.

Model Validation. Sneddon and Elliot (1946) derived analytical expressions of the additional normal and shear stresses vs. the distance normal to the fracture for two geometries: semi-infinite (Fig. 2) and penny-shaped fractures **(Fig. 3).**

The results of the 3D numerical model were compared to analytical solutions by plotting the additional stress in the direction parallel (ΔS_{yy}) and perpendicular (ΔS_{xx}) to the fracture as a function of the net extension pressure (p_{net}). The net extension pressure is the stress remaining as the fracture closes on the proppant minus the minimum horizontal stress. In the present study, net pressure is assumed to be constant along the fracture (uniform proppant distribution). Stress distributions are plotted vs. the distance normal to the fracture face (x) normalized by the fracture half-height (h_f).

Figs. 2 and 3 show that the additional stress in the horizontal plane is always higher in the direction perpendicular to the fracture than in the direction parallel to the fracture. As is true initially, the direction of maximum horizontal stress is parallel to the crack, and the stresses are reoriented in the vicinity of the fracture. The numerical results agree well with the analytical solution, indicating that the numerical results are correct for this simple case.

The additional stress normal to the fracture (ΔS_{xx}) decreases monotonically with distance away from the fracture. For the case of the penny-shaped fracture (Fig. 3), ΔS_{yy} becomes negative at some distance normal to the fracture and then passes through a minimum.

Comparison of Stress Reorientation Because of Poroelastic and Mechanical Effects. Stress reorientation around fractured wells can occur because of the fracture opening and because of poroelastic effects. Because the production or injection of fluids is minimal, poroelastic effects can be neglected in the fracturing of horizontal wells. However, in other cases where significant volumes of fluids have been produced from a well, poroelastic effects can be dominant.

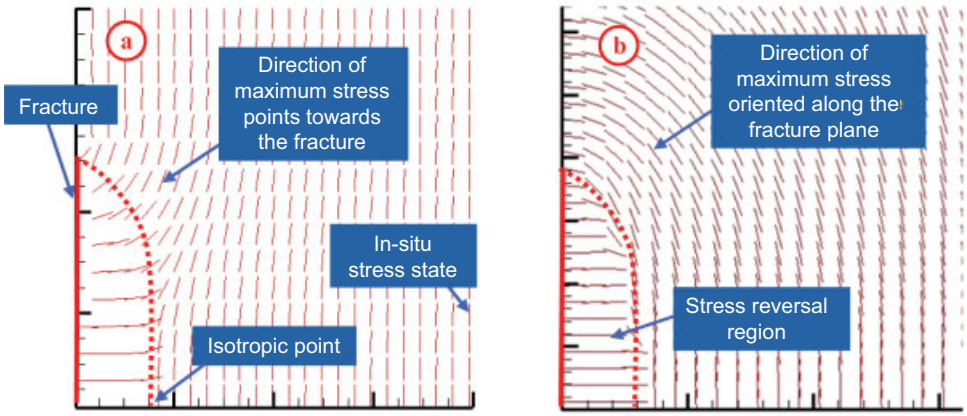

Fig. 4—Comparison of stress reorientation because of (a) mechanical effects and (b) poroelastic effects (direction of maximum horizontal stress).

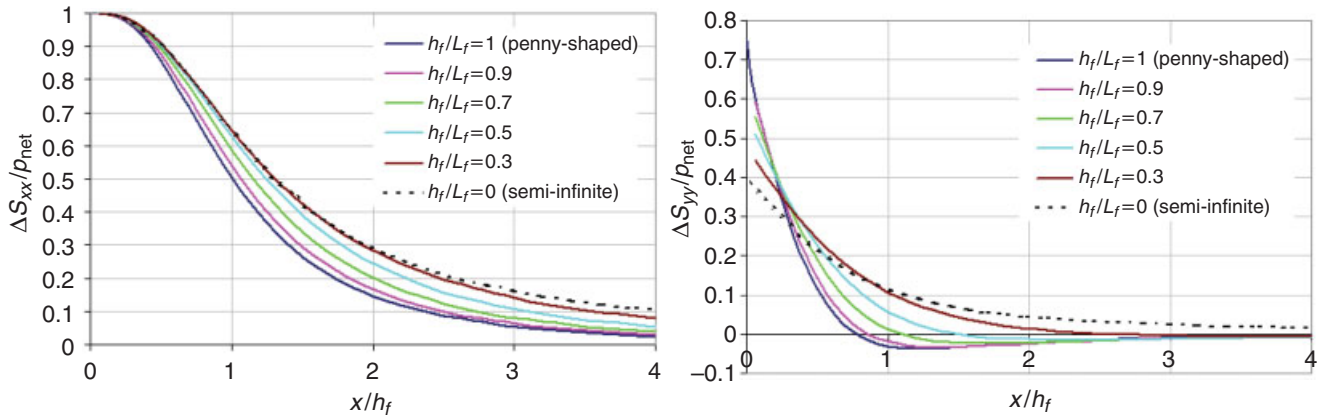

Fig. 5—Effect of fracture aspect ratio (h_f/L_f) on the stress perturbation.

The structure of stress reorientation around a single fracture because of poroelastic effects has been well described in the literature (Siebrits et al. 1998; Singh et al. 2008; Roussel and Sharma 2010). In the vicinity of the fracture, the direction of maximum horizontal stress is rotated 90° from its in-situ direction (for producing wells). Stress reorientation is not just limited to the stress-reversal region. The stress distribution resulting from the mechanical opening of a fracture differs from that because of poroelastic stresses. It was shown that outside the stress reversal region, the direction of maximum horizontal stress points toward the fracture (radial orientation), while it is oriented in the orthoradial direction in the case of poroelastic effects (Roussel and Sharma 2010) **(Fig. 4).**

The extent of the stress-reversal region (L_f') is not limited to 0.58 L_f, which has been shown numerically by Siebrits et al. (1998) to be the highest possible value of L_f' because of poroelastic effects. It may even extend to a distance larger than the fracture half-length (L_f). How far the stress-reversal region extends in the reservoir depends mainly on fracture width and height and on the Young's modulus in the pay zone. The reoriented-stress region (outside the stress-reversal region) is confined to the vicinity of the fracture, contrary to poroelastic stress reorientation, which can be observed far inside the reservoir.

Effect of Fracture Dimensions. The additional stresses in the parallel and normal directions are plotted vs. the dimensionless distance x/h_f normal to the fracture in **Fig. 5.** Both components increase as the fracture length increases compared to its height. The quantity of practical interest, though, is the difference between the additional stress in the direction perpendicular to and in the direction parallel to the fracture **(Fig. 6).** This difference represents the stress contrast that is generated by the opening of the fracture, or the generated stress contrast (GSC):

$$GSC = \Delta S_{\perp} - \Delta S_{//} = \Delta S_{xx} - \Delta S_{yy}. \quad \ldots\ldots\ldots\ldots\ldots\ldots\ldots\ldots (5)$$

In most situations, the creation of the fracture generates large additional stresses perpendicular to the fracture face. This alters the stress contrast and may cause the direction of maximum stress to rotate 90° in the vicinity of the fracture. The stress contrast generated by the open crack decreases with distance from the fracture (Fig. 6). At some distance from the fracture, this stress contrast becomes smaller than the in-situ stress contrast and the direction of maximum stress is oriented as initially.

The areal extent of the stress-reversal region is directly proportional to the fracture height because the distance to the fracture is normalized by the fracture half-height in our analysis. Fig. 6 also shows that as the fracture length increases, the GSC is higher. For instance, assuming that the in-situ stress contrast is equal to 0.2 p_{net}, the maximum distance of stress reversal L_f' is increased by 36% for a semi-infinite fracture compared to a penny-shaped fracture (Fig. 6).

Effect of Poisson's Ratio in the Pay Zone. The effect of the Poisson's ratio in the pay zone on the stress reorientation around the fracture depends on the fracture geometry. In the limiting case

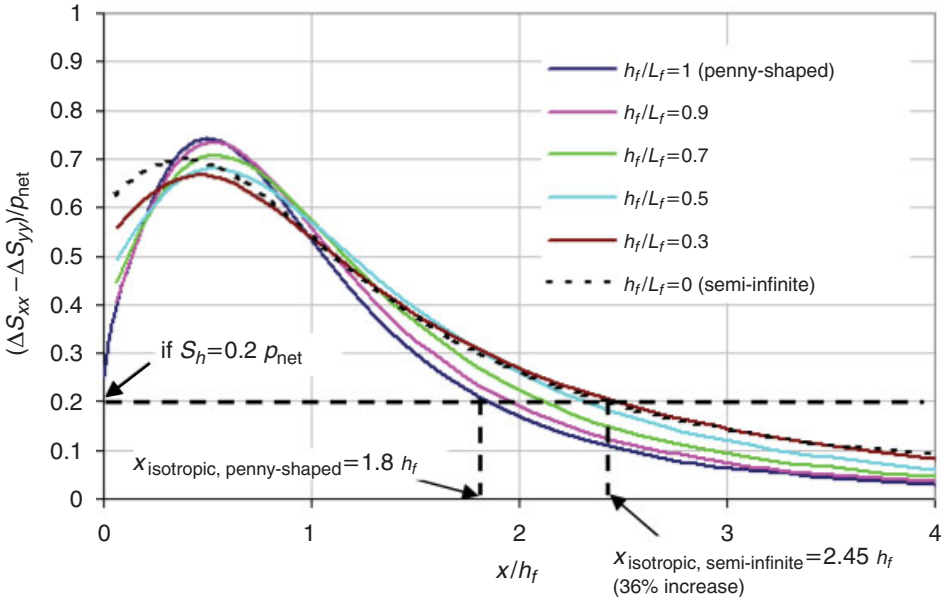

Fig. 6—Effect of fracture aspect ratio (h_f/L_f) on the GSC.

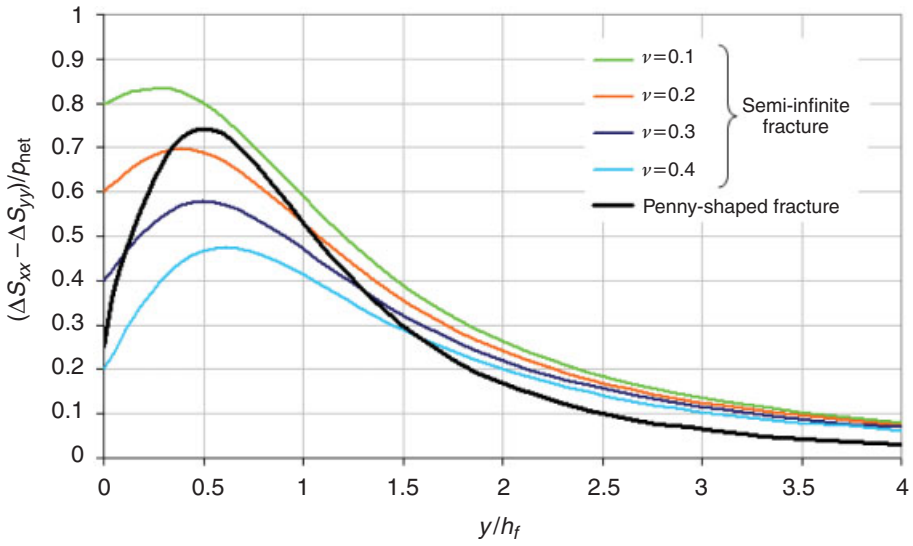

Fig. 7—Effect of Poisson's ratio in the pay zone on the GSC for semi-infinite and penny-shaped fractures.

of a penny-shaped fracture ($h_f = L_f$), stresses are independent of the Poisson's ratio (Sneddon and Elliot 1946), and so is the GSC. In the more general case where the fracture length differs from the fracture height, Poisson's ratio will play a role.

It is shown in **Fig. 7** that an opened crack generates more stress contrast in a rock with a low Poisson's ratio. A low Poisson's ratio implies that the deformation in the direction parallel to the fracture is small compared to the deformation in the direction normal to the fracture. When $\nu_p = 0$, all the deformation occurs along the in-situ direction of minimum horizontal stress ($\varepsilon_{yy} = 0$), thus maximizing the stress contrast generated.

Effect of the Bounding Layers' Mechanical Properties. Models of stress interference available in the literature (Sneddon and Elliot 1946; Cheng 2009) assume homogeneous mechanical properties and do not model layered rocks accurately. The rocks bounding gas reservoirs often have mechanical properties different from those of the reservoir and can play an important role in stress reorientation. **Fig. 8** shows that the GSC decreases if the Young's modulus of the bounding layers is higher than in the pay zone. The effect of the bounding layers' Young's modulus was analyzed for a fracture-penetration factor h_p/h_f equal to 0.75. The width of an opened crack is proportional to the Young's modulus. The relationship between maximum fracture width w_0 (at the center of the fracture) and net pressure for a semi-infinite fracture is given in Eq. 6 (Palmer 1993). If the fracture penetrates into a weaker bounding layer (lower Young's modulus), the fracture width is affected negatively **(Fig. 9).** Thus, a smaller stress contrast is generated by the fracture.

$$w_0 = \frac{4\left(1-\nu^2\right)}{E} p_{net} h_f. \quad \ldots\ldots\ldots\ldots\ldots\ldots\ldots\ldots\ldots\ldots (6)$$

The effect of the Poisson's ratio in the bounding layers was also analyzed **(Fig. 10).** It is shown that the GSC is independent of this value, and it depends only on the Poisson's ratio inside the pay zone.

Effect of Fracture Containment. The bounding layers' mechanical properties do not affect the extent of stress reorientation if the fracture is fully contained. In the Barnett shale, fractures are generally well contained in the pay zone even though "out-of-zone" growth has been measured in the field (Maxwell et al. 2002). From the relationship between fracture width and Young's modulus (Eq. 6), it can be deduced that the further the fracture penetrates into the bounding layers, the more the stress reorientation will be affected by their mechanical properties. For instance, in the case where the Young's modulus is higher in the layers bounding the pay zone, the maximum width of the crack, and consequently the GSC, decreases as the fracture height increases (Figs. 9 and 10).

Application of the Model to Multiple Hydraulic Fractures in Horizontal Wells

The quantification of the extent of the stress-reversal region around a propped-open fracture is critical in the design of multiple hydraulic fractures in horizontal wells. In low-permeability reservoirs such as shales where the slow depletion allows for short spacing

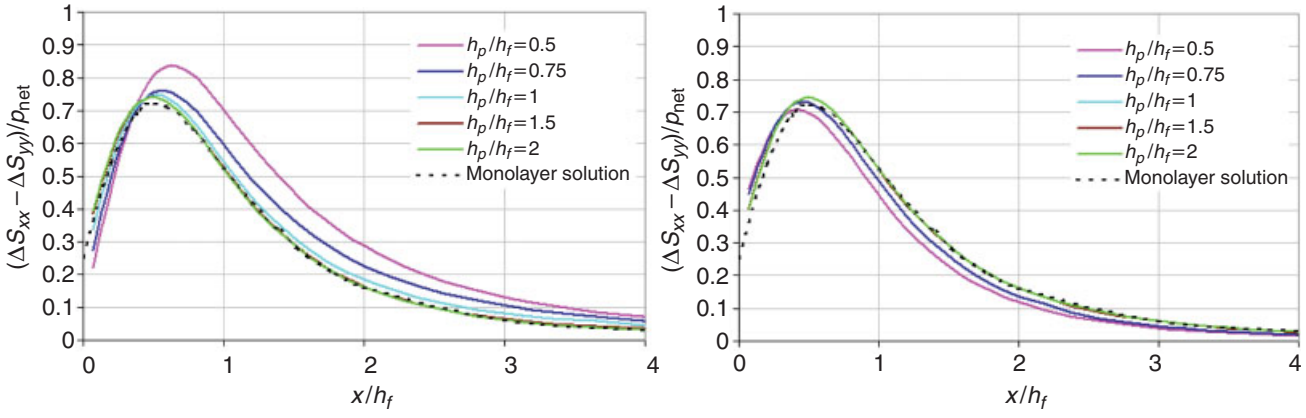

Fig. 8—Effect of fracture penetration on the GSC for a penny-shaped fracture (h_f/L_f = 1) and (a) E_b/E_p = 0.6, (b) E_b/E_p = 3.

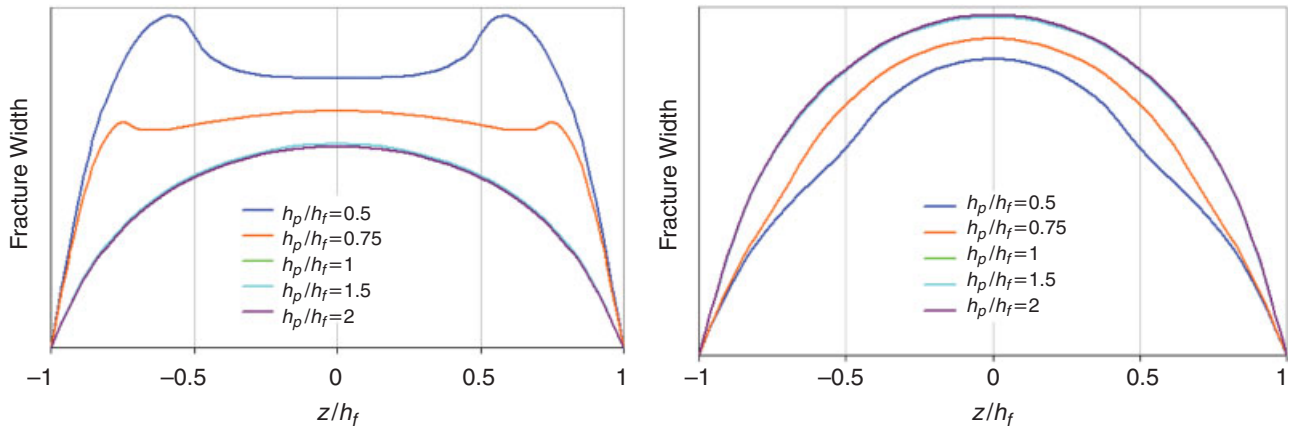

Fig. 9—Effect of fracture penetration on fracture width for a penny-shaped fracture (h_f/L_f = 1) and (a) E_b/E_p = 0.6, (b) E_b/E_p = 3.

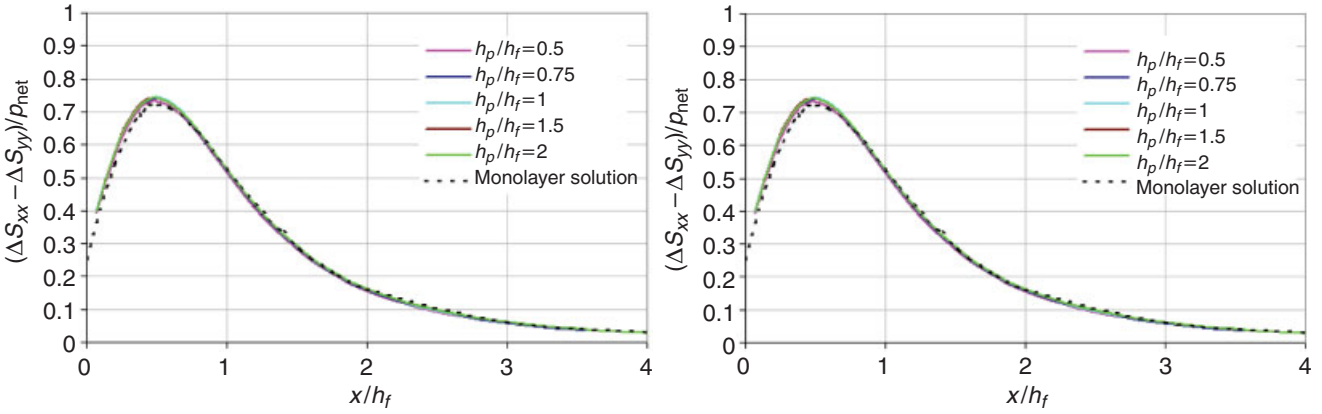

Fig. 10—Effect of fracture penetration on the GSC for a penny-shaped fracture (h_f/L_f = 1) and (a) ν_b/ν_p = 2, (b) ν_b/ν_p = 0.67.

between sequential fractures, great attention should be given to avoid stress interference between transverse fractures. The model of mechanical-stress reorientation presented in the previous section of the paper is applied to the case of the Barnett shale. Values of the reservoir and fracture parameters are provided in **Table 1.** The dimensions of the opened cracks (height, length, and width) are similar for all fractures.

Poroelastic effects because of the leakoff of the fracturing fluid into the reservoir are neglected in this study because of the very low permeability of the shale and the small amount of fluid leakoff during fracturing.

TABLE 1—RESERVOIR PARAMETERS FOR BARNETT SHALE GAS WELL

Pay zone Young's Modulus E_p (psi)	$7.3.10^6$
Bounding layer Young's Modulus E_b (psi)	$3.0.10^6$
Poisson's Ratio v	0.2
S_{hmax} (psi)	6400
S_{hmin} (psi)	6300
Depth (ft)	7000
Pay zone half-thickness h_p (ft)	150
Fracture half-height h_f (ft)	150
Fracture half-length L_f (ft)	500
Fracture maximum width w_0 (mm)	4

Definition of the Minimum Fracture Spacing. As can be seen in **Fig. 11,** a stress reorientation of 90° occurs within a certain region of the rock. The minimum fracture spacing can be defined as the distance between the fracture and the end of the stress-reversal region, also known as the isotropic point. This is shown as S_{90} in Fig. 11. No refracturing should be generated within S_{90}. In this stress-reversal region, the direction of maximum horizontal stress is parallel to the horizontal well, which would lead the refracture either to grow longitudinal to the well or to screen out because the change in fracture orientation is very rapid. The gain in production and new reserves will be very limited.

Even when refracturing is performed past S_{90}, refracture propagation is affected by previous fractures. If a fracture is initiated just outside of the stress-reversal region, it will propagate away from the previous fracture, following the direction of maximum horizontal stress. This fracture reorientation decreases as fracture spacing increases. The distances between subsequent fractures needed to limit fracture deviations from the orthogonal plane to less than 5° and 10° are defined, respectively, as S_5 and S_{10} (Fig. 11). Note that the presence of natural fractures and their effect on fracture propagation are not modeled. In the situation where the natural fractures are mainly oriented perpendicular to the direction of maximum horizontal stress (as in the Barnett shale), the direction of propagation of hydraulic fractures may deviate significantly from the preferential direction, in particular when stress anisotropy is low (Olson 2008).

In very-low-permeability reservoirs such as the Barnett shale, it is desirable to minimize fracture spacing while at the same time ensuring transverse fracture growth to access gas in the reservoir efficiently. This implies that the optimal fracture spacing should be just beyond the S_5 contour.

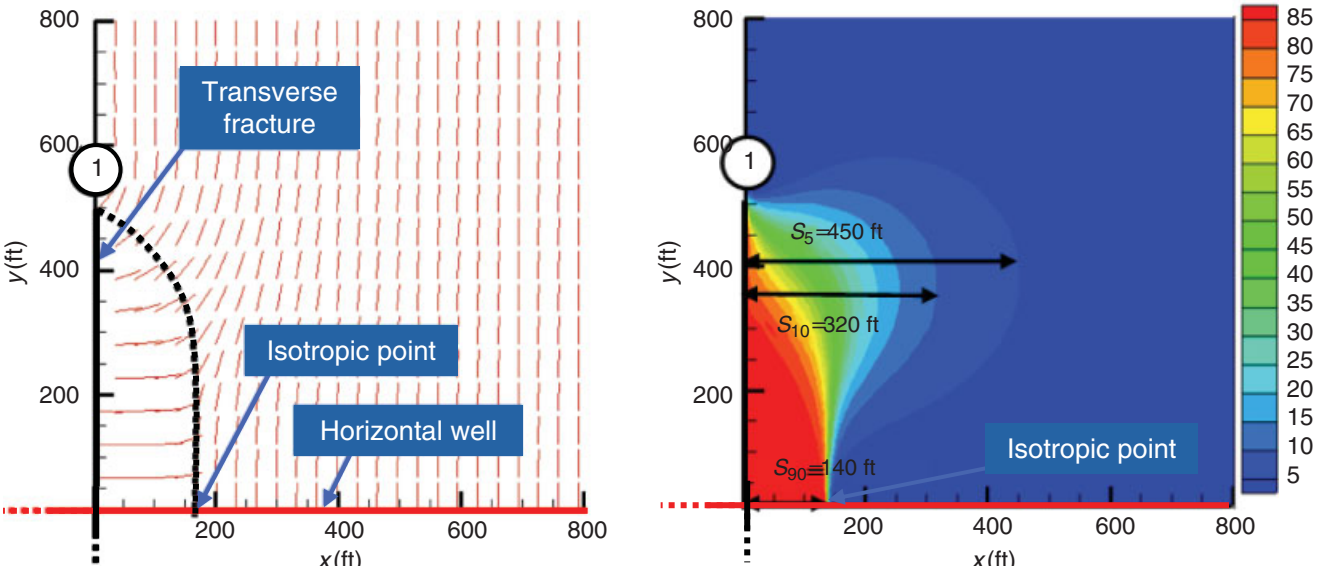

Fig. 11—Direction of maximum horizontal stress and angle of stress reorientation for a single transverse fracture.

Sequential Fracturing. The stress interference caused by one transverse fracture is shown in Fig. 11. However, horizontal wells are fractured multiple times. Thus, the values for the minimum fracture spacing provided in Fig. 11 are underestimates (S_{90} = 140 ft, S_{10} = 320 ft, and S_5 = 450 ft). The stress perturbation caused by each fracture is cumulative with the effect of all prior fractures. Therefore, stress interference (or reorientation) increases with the number of fractures and also depends on the sequence of fracturing. In this section, we will investigate and compare two fracturing sequences **(Fig. 12):** (a) a conventional consecutive fracturing from toe to heel, (b) sequencing the fractures alternately, and (c) simultaneously fracturing two adjacent wells.

Effect of Fracture Width and In-Situ Stress Contrast. Commonly accepted values for the propped-fracture width (Palisch et al. 2008) and the horizontal-stress contrast (Weng and Siebrits 2007) in the Barnett shale are 4 mm and 100 psi, respectively (Table 1). As the fracture width increases, the stress contrast generated by the propped-open fracture increases. Thus, depending on the horizontal contrast present in situ and the fracture design, the stress interference caused by the opening of multiple fractures will be affected. In **Fig. 13,** the distance between the fracture and the isotropic point (minimum fracture spacing S_{90}) is plotted against fracture width for different values of the in-situ stress contrast.

Consecutive Fracturing (1-2-3-4-5…). When a horizontal well is consecutively fractured, the stress perturbation ahead of the latest fracture increases with each additional fracture (Soliman and Adams 2004) until it reaches a maximum. This maximum state of stress reorientation in turn depends on the fracture spacing. The spacing between multiple transverse fractures has been adjusted so that the maximum value taken by S_{90} (extent of the stress-reversal region) remains inferior to the fracture spacing **(Fig. 14).** The calculation of the stress perturbation ahead of the last fracture (n + 1) of Fig. 14 provides a good estimate of the maximum state of stress reorientation when taking into account the effect of multiple transverse fractures **(Fig. 15).** The spacing quantities corresponding to the maximum state of stress reorientation are summarized below:

$$\begin{cases} S_{90} = 230 \text{ ft} \\ S_{10} = 430 \text{ ft} \\ S_5 = 600 \text{ ft} \end{cases}$$

In order to limit refracture deviation, the horizontal well corresponding to the values given in Table 1 should be refractured every 430 to 600 ft, which is equal to 1.4 to 2 fracture heights. This calculation corroborates typical values of the recommended fracture spacing from field experience (Ketter et al. 2008).

Alternate Fracturing Sequence (1-3-2-5-4…). If the sequence of fracture placement was altered to conduct fractures in the sequence 1-3-2-5-4, it is shown here that the fractures could be placed much closer to each other. This proximity helps to drain the reservoir most efficiently by ensuring that the fractures remain transverse. We recognize that this fracturing sequence may not be possible with current downhole tools and that special tools may need to be developed. However, our goal is to demonstrate the significant benefits of this alternate fracturing sequence compared with the sequential fractures currently being pumped.

The new strategy consists of placing the second fracture at the location of what traditionally would be the third fracture. Perforations for the second fracture are placed at a distance greater than S_5.

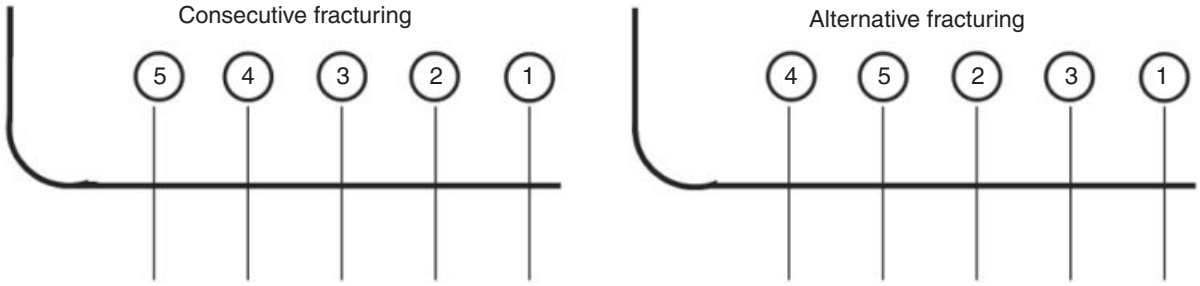

Fig. 12—Two fracturing sequences: (a) consecutive (1-2-3-4-5) and (b) alternate (1-3-2-5-4).

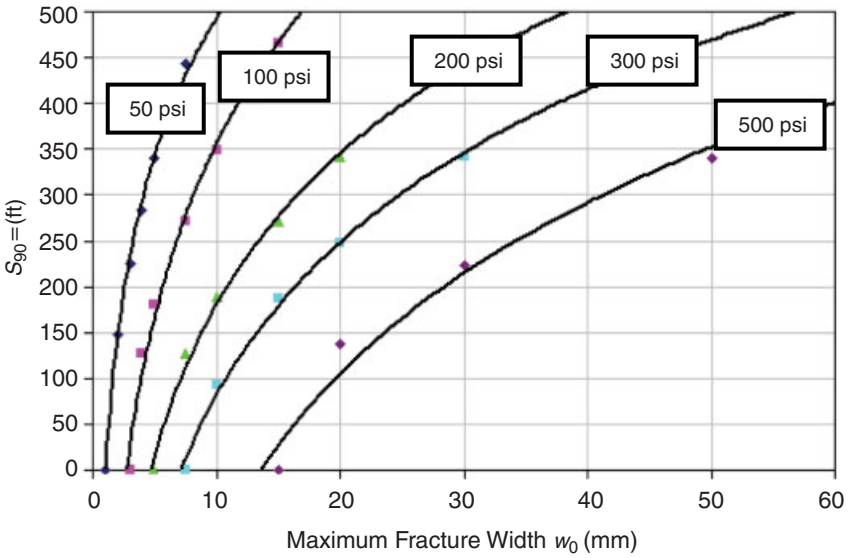

Fig. 13—Minimum fracture spacing S_{90} vs. maximum fracture width for different values of the horizontal-stress contrast.

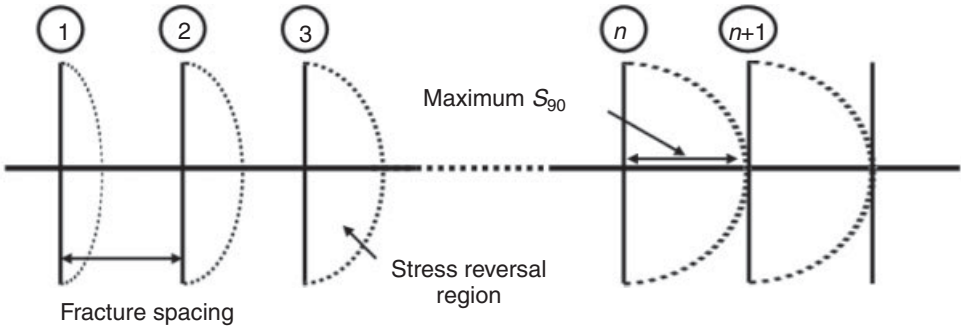

Fig. 14—Modeling of maximum stress reorientation because of multiple consecutive fractures in a horizontal well.

This ensures that its deviation from a transverse or perpendicular trajectory is minimal. In the first calculation (600-ft spacing) **(Fig. 16),** the direction of maximum horizontal stress is reversed along the whole interval separating the fractures. When the fracture spacing is increased to 650 ft, there is an interval where the stress distribution will force the third fracture to grow along a normal path intersecting the horizontal well at the middle point between previous fractures, where the reorientation angle is exactly equal to zero **(Fig. 17).** However, the width of the acceptable interval for the new perforations is extremely narrow (20 ft). For a 700-ft

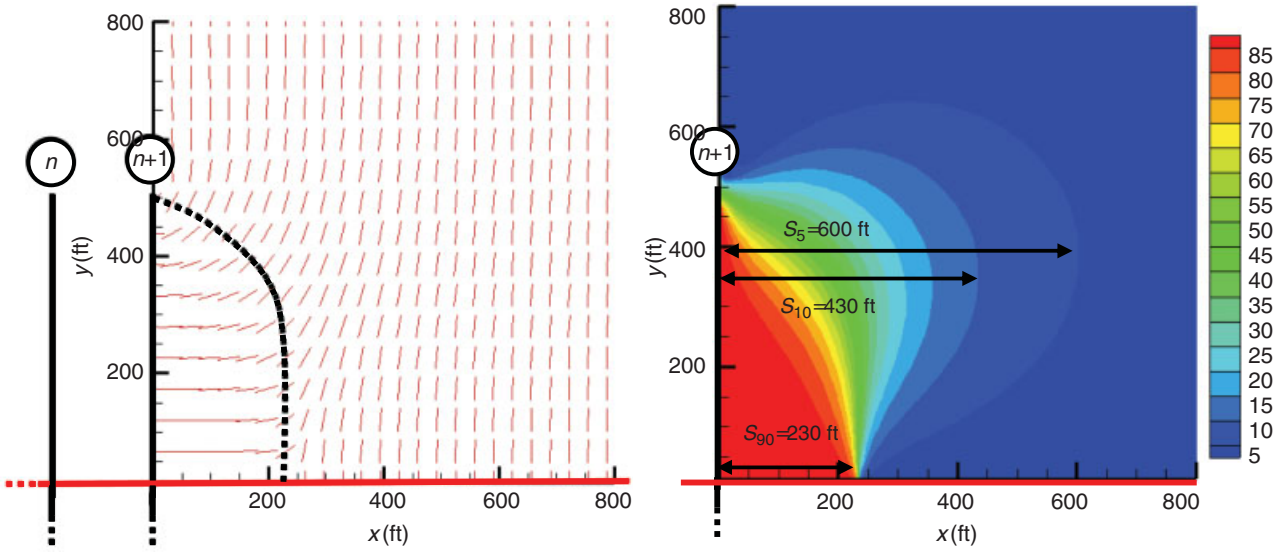

Fig. 15—Maximum stress reorientation from multiple transverse fractures (direction of maximum horizontal stress and angle of stress reorientation).

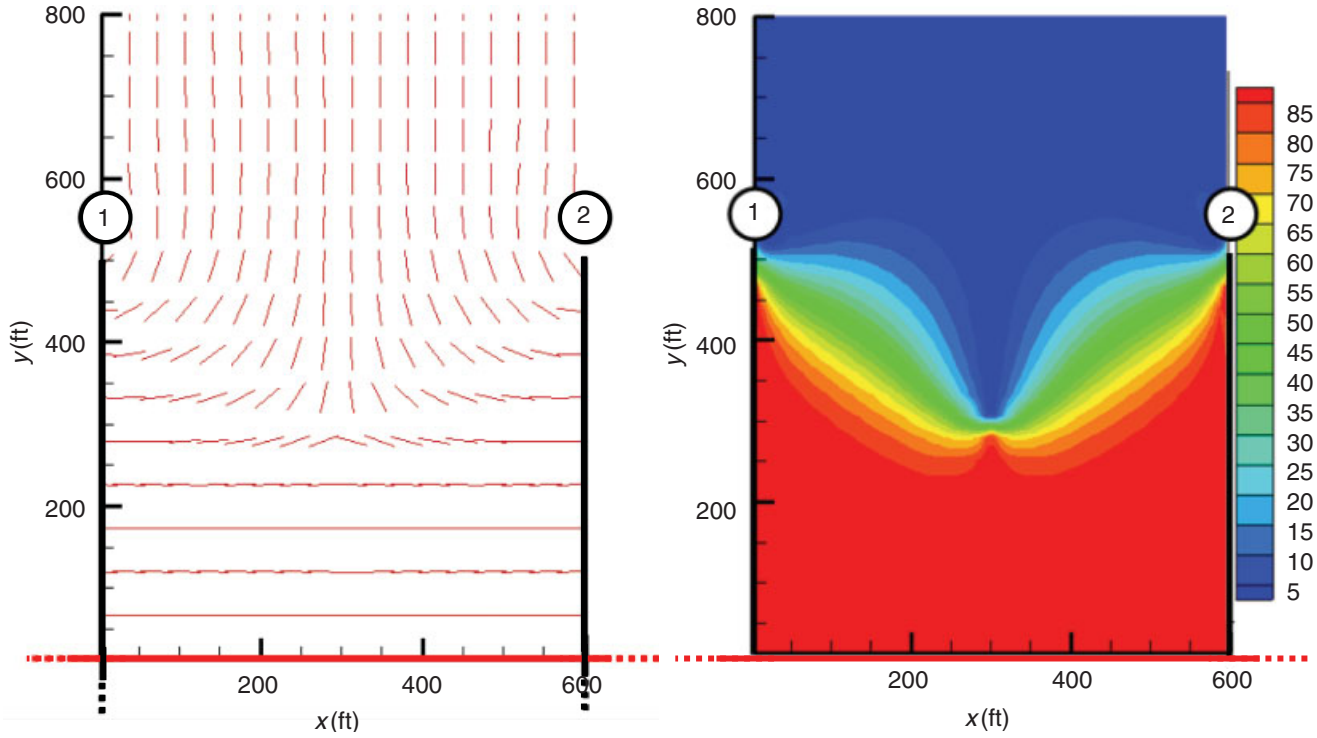

Fig. 16—Direction of maximum horizontal stress and angle of stress reorientation for a fracture spacing of 600 ft.

spacing, the width of the refracturing interval is considerably increased (220 ft) **(Fig. 18).** If the third fracture were to be initiated in this interval, the stress reorientation would favor transverse fracture growth. The location of this third fracture does not have to be exactly at the midpoint between the previous fractures. In fact, even if the fracture is initiated at some distance from the middle, it will follow a trajectory (as seen in the stress profiles; see Fig. 18) that will force it to grow along the midplane between the previous fractures.

For the last simulation, the fracture spacing is equal to 350 ft (1.17 times the fracture height), which is smaller than the recommended value for consecutive fracturing (S_5 = 600 ft). The practical advantage of this fracturing sequence, in addition to the fact that minimum fracture spacing is decreased compared with consecutive fracturing, is that stress reorientation is playing to our advantage, forcing the middle fracture to propagate in the optimum direction.

Impact of Adjacent Wells (Zipper Fracs). The technique of zipper fracs consists of simultaneously fracturing two parallel horizontal wells. In the particular case that was modeled, the spacing between adjacent wells is equal to the fracture length.

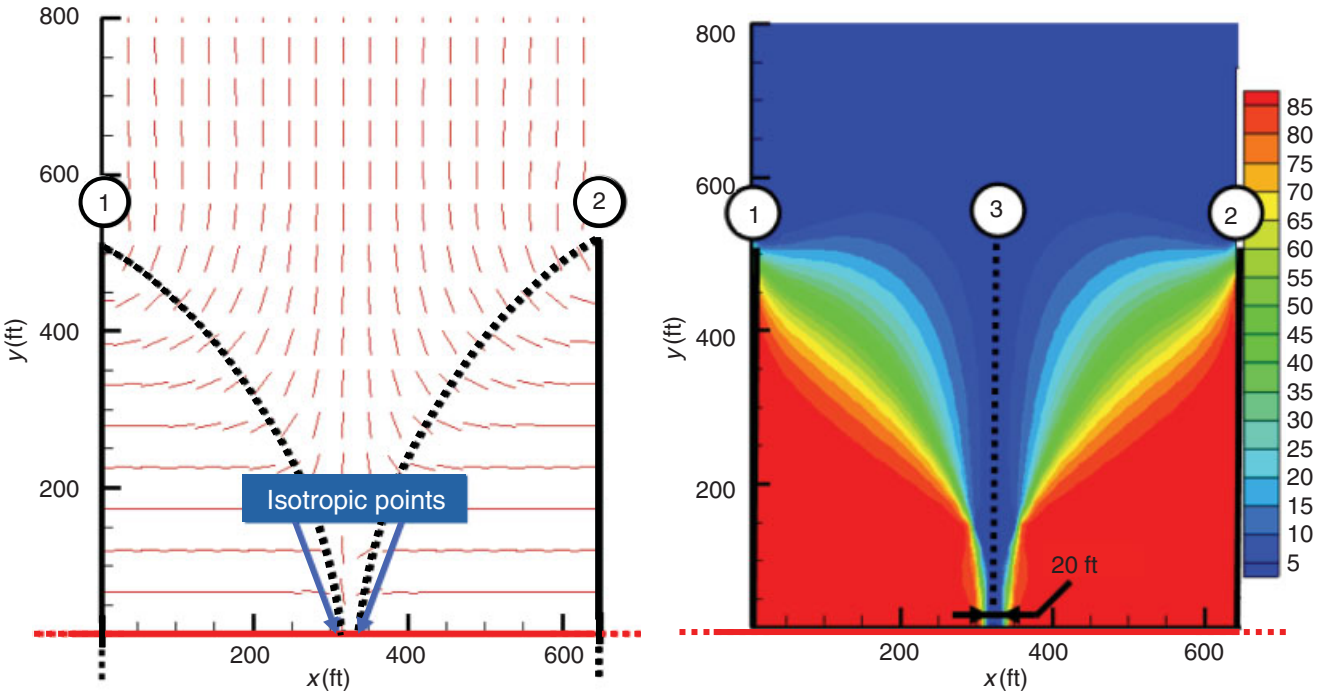

Fig. 17—Direction of maximum horizontal stress and angle of stress reorientation for a fracture spacing of 650 ft.

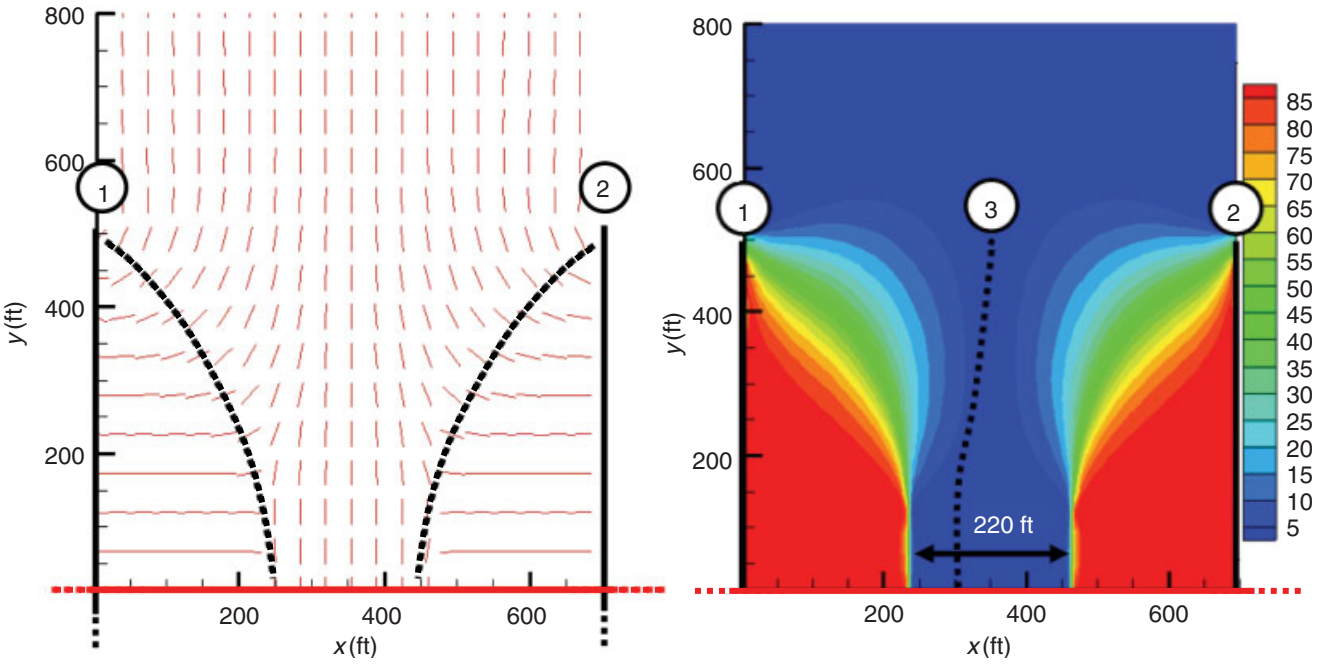

Fig. 18—Direction of maximum horizontal stress and angle of stress reorientation for a fracture spacing of 700 ft.

The maximum state of stress reorientation for zipper fracs was calculated following the same procedure as for a single well (Fig. 14). Compared with consecutive fracturing of a single well, the fracture spacing needed to minimize fracture deviation (S_{10}, S_5) is significantly reduced **(Fig. 19):**

$$\begin{cases} S_{90,\ \text{zipper-fracs}} = 230\ \text{ft} \\ S_{10,\ \text{zipper-fracs}} = 330\ \text{ft} = 77\%\ S_{10,\ \text{singlewell}} \\ S_{5,\ \text{zipper-fracs}} = 400\ \text{ft} = 67\%\ S_{5,\ \text{singlewell}} \end{cases}$$

It is shown that the extent of stress reversal around zipper fracs is unchanged compared with the case of the single well (S_{90} = 230 ft). However, the reoriented zone outside the stress-reversal region shrank significantly (S_{10} = 330 < 430 ft and S_5 = 400 < 600 ft). This is because of the symmetry along the plane x = 500 ft (middle plane between adjacent wells), where the reorientation angle is equal to zero.

Conclusions

A comprehensive and quantitative study of stress reorientation around fractured horizontal wells has been presented. A 3D

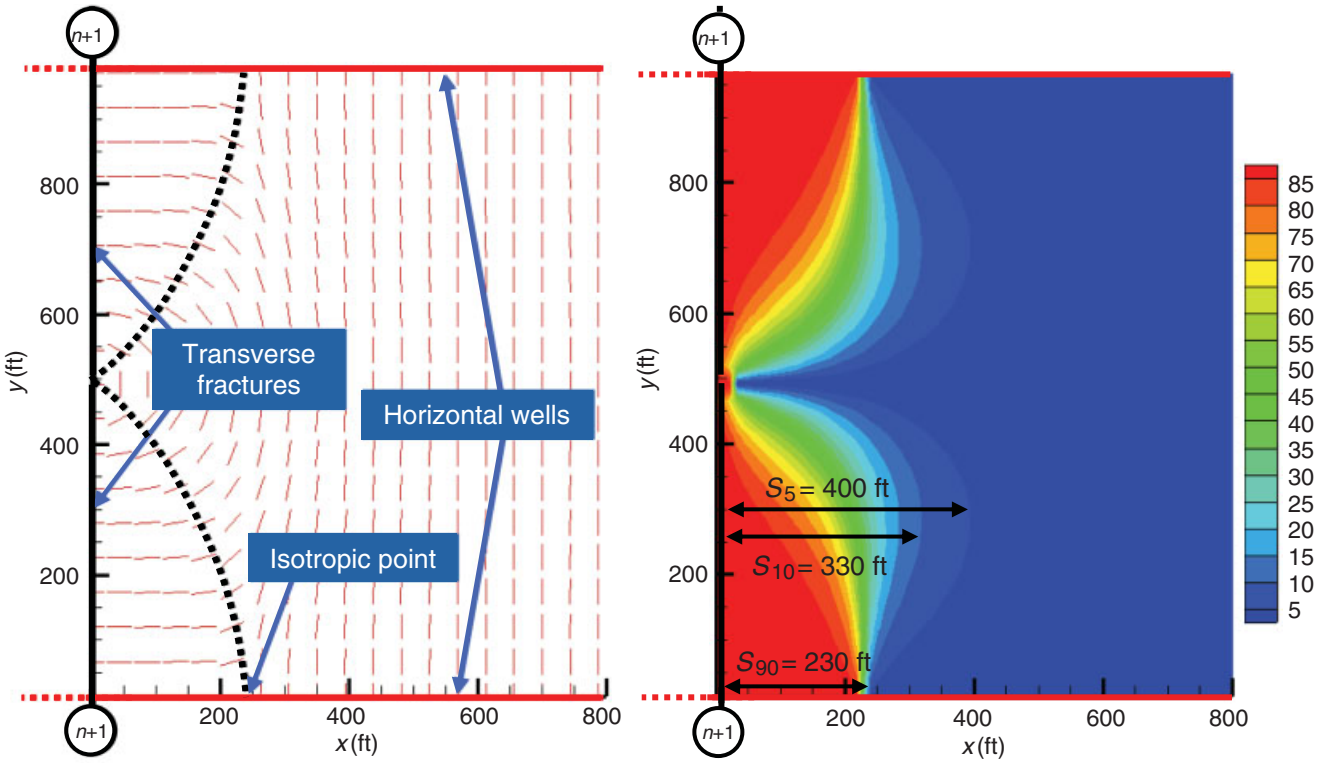

Fig. 19—Maximum stress reorientation from multiple pairs of transverse fractures (direction of maximum horizontal stress and angle of stress reorientation).

TABLE 2—COMPARISON OF MINIMUM AND RECOMMENDED FRACTURE SPACING FOR DIFFERENT FRACTURING TECHNIQUES FOR A BARNETT SHALE FIELD CASE

	Consecutive Fracturing (1-2-3-4-5…)	Alternate Fracturing (1-3-2-5-4…)	Simultaneous Fracturing of Adjacent Wells (Well Spacing = 2 L_f)
Minimum fracture spacing (ft) (= S_{90} or interval for 3rd frac > 0 ft)	230	325	230
Recommended fracture spacing (ft) (= S_5 or interval for 3rd frac > 100 ft)	600	340	400

numerical model was used to take into account the presence of layers bounding the pay zone as well as fracture containment. It was shown that the stress contrast generated by the opening of a propped fracture is a function of the fracture dimensions (w_0, h_f, L_f), the Poisson's ratio in the pay zone (ν_p), the ratio of Young's moduli of the bounding layers and the reservoir (E_b/E_p), and the fracture penetration into the bounding layers (h_f/h_p).

On the basis of the simulation results obtained, we can summarize our recommendations as follows:

- To avoid longitudinal fractures, the minimum fracture spacing must be larger than S_{90}. The model presented here allows us to obtain reliable estimates of S_{90} for a given set of reservoir and fracture properties.
- To ensure transverse fractures and avoid deviation of the fracture from its orthogonal path, the fracture spacing should be larger than S_5, which can be calculated from the model.
- The alternative fracturing technique proposed here allows the fracture spacing needed to ensure transverse fractures to be reduced by almost 50% (Fig. 17). Values of the minimum and recommended fracture spacing are given in **Table 2,** using the Barnett shale as an example.

The model presented in this paper can be used to estimate values of the minimum and optimum fracture spacing in horizontal wells for a given set of reservoir properties and a proposed fracture design. Values for the recommended fracture spacing for an example case of the Barnett shale are presented in Table 2 for three possible fracturing sequences: (a) consecutive fracturing, (b) alternative fracturing, and (c) simultaneous fracturing of adjacent wells. The last two techniques make it possible to shrink the stress-reorientation region, thus significantly reducing the fracture spacing needed to limit fracture deviation from the desired orthogonal path. A technique that consists of sequencing the fractures in an alternative order results in the smallest fracture spacing (340 ft). It also presents the important advantage of forcing the "middle fracture" to propagate along the orthogonal plane midway between the previous two fractures. The development of technologies allowing this fracturing technique to be applied in the field may prove beneficial to the performance of stimulation treatments in horizontal wells.

Acknowledgments

The authors would like to acknowledge the financial support provided by the Department of Energy / RPSEA and the companies supporting the Fracturing and Sand Control Joint Industry Project at the University of Texas at Austin (Anadarko, BP, BJ Services, ConocoPhillips, Halliburton, Shell, Schlumberger, and Total).

Nomenclature

E_b = Young's modulus of the bounding layers
E_p = Young's modulus of the pay zone
G = shear modulus
h_f = fracture half-height
h_p = pay-zone half-thickness
K = dry bulk modulus
L_f = fracture half-length
p_{net} = net extension pressure
S_{hmax} = maximum horizontal in-situ stress
S_{hmin} = minimum horizontal in-situ stress
S_V = vertical in-situ stress
S_5 = distance between fracture and end of 5° stress-reorientation region
S_{10} = distance between fracture and end of 10° stress-reorientation region
S_{90} = distance between fracture and isotropic point (=L_f')
ν_b = Poisson's ratio in the bounding layers
ν_p = Poisson's ratio in the pay zone
w_0 = maximum fracture width

References

Cheng, Y. 2009. Boundary Element Analysis of the Stress Distribution around Multiple Fractures: Implications for the Spacing of Perforation Clusters of Hydraulically Fractured Horizontal Wells. Paper SPE 125769 presented at the SPE Eastern Regional Meeting, Charleston, West Virginia, USA, 23–25 September. doi: 10.2118/125769-MS.

Cipolla, C.L., Lolon, E.P., Mayerhofer, M.J., and Warpinski, N.R. 2009. Fracture Design Considerations in Horizontal Wells Drilled in Unconventional Gas Reservoirs. Paper SPE 119366 presented at the SPE Hydraulic Fracturing Technology Conference, The Woodlands, Texas, USA, 19–21 January. doi: 10.2118/119366-MS.

Fisher, M.K., Heinze, J.R., Harris, C.D., Davidson, B.M., Wright, C.A., and Dunn, K.P. 2004. Optimizing Horizontal Completion Techniques in the Barnett Shale Using Microseismic Fracture Mapping. Paper SPE 90051 presented at the SPE Annual Technical Conference and Exhibition, Houston, 26–29 September. doi: 10.2118/90051-MS.

Ketter, A.A., Daniels, J.L., Heinze, J.R., and Waters, G. 2008. A Field Study Optimizing Completion Strategies for Fracture Initiation in Barnett Shale Horizontal Wells. *SPE Prod & Oper* **23** (3): 373–378. SPE-103232-PA. doi: 10.2118/103232-PA.

Maxwell, S.C., Urbancik, T.I., Steinsberger, N.P., and Zinno, R. 2002. Microseismic Imaging of Hydraulic Fracture Complexity in the Barnett Shale. Paper SPE 77440 presented at the SPE Annual Technology Conference and Exhibition, San Antonio, Texas, USA, 29 September–2 October. doi: 10.2118/77440-MS.

Mayerhofer, M.J., Lolon, E.P., Warpinski, N.R., Cipolla, C.L., Walser, D., and Rightmire, C.M. 2010. What Is Stimulated Reservoir Volume? *SPE Prod & Oper* **25** (1): 89-98. SPE-119890-PA. doi: 10.2118/119890-PA.

Mutalik, P.N. and Gibson, B. 2008. Case History of Sequential and Simultaneous Fracturing of the Barnett Shale in Parker County. Paper SPE 116124 presented at the SPE Annual Technical Conference and Exhibition, Denver, 21–24 September. doi: 10.2118/116124-MS.

Olson, J.E. 2008. Multi-fracture Propagation Modeling: Application to hydraulic fracturing in shales and tight gas sands. Paper ARMA 08-327 presented at the 42nd US Rock Mechanics Symposium, San Francisco, 29 June–2 July.

Olson, J.E. and Dahi-Taleghani, A. 2009. Modeling Simultaneous Growth of Multiple Hydraulic Fractures and Their Interaction With Natural Fractures. Paper SPE 119739 presented at the SPE Hydraulic Fracturing Technology Conference, The Woodlands, Texas, USA, 19–21 January. doi: 10.2118/119739-MS.

Palmer, I.D. 1993. Induced Stresses Due to Propped Hydraulic Fracture in Coalbed Methane Wells. Paper SPE 25861 presented at the Low Permeability Reservoirs Symposium, Denver, 26–28 April. doi: 10.2118/25861-MS.

Palisch, T.T., Vincent, M.C., and Handren, P.J. 2008. Slickwater Fracturing—Food for Thought. Paper SPE 115766 presented at the SPE Annual Technical Conference and Exhibition, Denver, 21–24 September. doi: 10.2118/115766-MS.

Roussel, N.P. and Sharma, M.M. 2010. Quantifying Transient Effects in Altered-Stress Refracturing of Vertical Wells. *SPE J.* **15** (3): 770–782. SPE-119522-PA. doi: 10.2118/119522-PA.

Siebrits, E., Elbel, J.L., Detourney, E., Detournay-Piette, C., Christianson, M., Robinson, B.M., and Diyashev, I.R. 1998. Parameters Affecting Azimuth and Length of a Secondary Fracture During a Refracture Treatment. Paper SPE 48928 presented at the SPE Annual Technical Conference and Exhibition, New Orleans, 27–30 September. doi: 10.2118/48928-MS.

Singh, V., Roussel, N.P., and Sharma, M.M. 2008. Stress Reorientation Around Horizontal Wells. Paper SPE 116092 presented at the SPE Annual Technical Conference and Exhibition, Denver, 21–24 September. doi: 10.2118/116092-MS.

Sneddon, I.N. and Elliot, H.A. 1946. The Opening of a Griffith Crack under Internal Pressure. *Quarterly of Applied Mathematics* **4** (3): 262–267.

Sneddon, I.N. 1946. The Distribution of Stress in the Neighbourhood of a Crack in an Elastic Solid. *Proc. R. Soc. Lond. A* **187** (1009): 229–260.

Soliman, M.Y. and Boonen, P. 1997. Review of Fractured Horizontal Wells Technology. Paper SPE 36289 presented at the Abu Dhabi International Petroleum Exhibition and Conference, Abu Dhabi, UAE, 13–16 October. doi: 10.2118/36289-MS.

Soliman, M.Y. and Adams, D. 2004. Geo-Mechanics Aspects of Multiple Fracturing of Horizontal and Vertical Wells. Paper SPE 86992 presented at the SPE International Thermal Operations and Heavy Oil Symposium and Western Regional Meeting, Bakersfield, California, USA, 16–18 March. doi: 10.2118/86992-MS.

Waters, G., Dean, B., Downie, R., Kerrihard, K., Austbo, L., and McPherson, B. 2009. Simultaneous Hydraulic Fracturing of Adjacent Wells in the Woodford Shale. Paper SPE 119635 presented at the SPE Hydraulic Fracturing Technology Conference, The Woodlands, Texas, USA, 19–21 January. doi: 10.2118/119635-MS.

Weng, X. and Siebrits, E. 2007. Effect of Production-Induced Stress Field on Refracture Propagation and Pressure Response. Paper SPE 106043 presented at the SPE Hydraulic Fracturing Technology Conference, College Station, Texas, USA, 29–31 January. doi: 10.2118/106043-MS.

Nicolas P. Roussel is a PhD candidate in the Department of Petroleum and Geosystems Engineering at The University of Texas at Austin. His research is focused on the modeling of stress reorientation and its application to the optimization of stimulation and restimulation operations. He has also published a journal article in the field of fluid suspensions. Roussel holds an MS degree in mechanical engineering from the Georgia Institute of Technology and a diplôme d'ingénieur from Arts et Métiers ParisTech in France. He is a member of SPE and the founder of the Petroleum Graduate Student Association at The University of Texas at Austin. He is being nominated for the 2011 Cedric K. Ferguson Medal. **Mukul M. Sharma** is professor and holder of the "Tex" Moncrief Chair in the Department of Petroleum and Geosystems Engineering at The University of Texas at Austin, where he has been for 25 years. He served as chairman of the department from 2001 to 2005. His current research interests include improved oil recovery, injection water management, hydraulic fracturing, formation damage, and petrophysics. He has published more than 200 journal articles and conference proceedings and holds 14 patents. Sharma holds a BTech degree in chemical engineering from the Indian Institute of Technology and MS and PhD degrees in chemical and petroleum engineering from the University of Southern California. Among his many awards, Sharma is the recipient of the 2009 Lucas Gold Medal, the 2004 SPE Faculty Distinguished Achievement Award, the 2002 Lester C. Uren Award, and the 1998 SPE Formation Evaluation Award. He served as an SPE Distinguished Lecturer in 2002, has served on the editorial boards of many journals, and has taught and consulted for the industry worldwide.